Journal of the Korean Society of Oceanography
Vol. 39, No. 1, pp. 35 — 45 March 2004

# Simulation of the Temperature and Salinity Along 36°N in the Yellow Sea with a Wave-Current Coupled Model

FANGLI QIAO, JIAN MA, YONGZENG YANG AND YELI YUAN
*The First Institute of Oceanography, State Oceanic Administration (SOA), Qingdao, China*
*Key Laboratory of Marine Science and Numerical Modeling (MASNUM), SOA, China*

Based on the MASNUM wave-current coupled model, the temperature and salinity structures along 36°N in the Yellow Sea are simulated and compared with observations. Both the position and strength of the simulated thermocline are similar to data analysis. The wave-induced mixing is strongest in winter and plays a key role in the formation of the upper mixed layer in spring and summer. Numerical experiments suggest that in the coastal area, wave-induced mixing and tidal mixing control the vertical structure of temperature and salinity.

**Key words:** Temperature, Salinity, The Yellow Sea, Wave-Current Coupled Model, Wave-Induced Mixing, Tidal mixing, Buoyance-Driven Mixing

## INTRODUCTION

The Yellow Sea is a semi-enclosed basin with the horizontal scale of 400 km by 1000 km (Fig. 1) and the maximal depth of 80 m. One of the most important features is the strong thermocline in summer that has been confirmed by many observations. However, all the coastal circulation models face some common problems including the weakness of the summer thermocline as well as the shallowness of the upper mixed layer (Martin, 1985; Kantha and Clayson, 1994; Ezer, 2000).

It is believed that the vertical mixing process which controls the structure of temperature and salinity can be separated into buoyance-driven and dynamic parts. In winter, the cooled surface water is denser than that below and buoyance-driven mixing quickly uniforms the density in vertical direction. This process is generally included in ocean models. The vertical dynamic mixing includes the following four processes:

1) Current turbulence mixing: Princeton Ocean Model (POM) employs the level 2.5 turbulence closure model to provide vertical mixing coefficients (Mellor and Yamada, 1982), which is one of the most important reasons why POM is widely accepted all over the world (Blumberg and Mellor, 1987; Ezer, 2000). Other methods, such as Prandtle mixing length theory (Fang and Ichiye, 1983), are also adopted to describe the current turbulence mixing;

2) Wave-induced mixing: Craig and Banner (1994) and Mellor (2001) analyzed the wave breaking mixing. Yuan et al. (1999) brought an idea to regard wave velocity as fluctuations of circulation. Based on the MASNUM wave number spectral model (Yuan *et al.*, 1991; Yang and Qiao, 2004), Qiao *et al.* (2004a) got the expression of wave-induced mixing and wave-induced Reynolds stress and developed the MASNUM wave-current coupled model;

3) Tidal mixing: Tide is so strong in the coastal sea that it can produce high vertical shearing strain of velocity, which will enhance the current turbulence mixing (Lee and Beardsley, 1999). The tidal mixing can be included by adding the tidal current in the circulation model or parameterizing the tidal effects (Yuan and Li, 1993). In this study, we prefer the former method;

4) Internal wave related mixing: Pacanowski and Philander (1981) gave a parameterization for the tropical area on Richardson number. Liungman (2000) developed the $\kappa$–$\varepsilon$ turbulence closure model. But in general, the ability to simulate the internal waves is on a preliminary stage (Yuan *et al.*, 2003), and their mixing effects need more research.

In this paper, the temperature and salinity in the Yellow Sea are simulated based on the MASNUM wave-current coupled model with tidal mixing. The

*Corresponding author: flgiao@21cn.com

following section describes the numerical models. Section 3 discusses comparisons between the observations and model results along 36°N. The last section is conclusion remarks.

## MODELS DESCRIPTIONS

### *Wave model*

This work employs the MASNUM (once called LAGFD-WAM) wave number spectral model (Yuan *et al.*, 1991) which has been validated many times by observations (Yu *et al.*, 1997) and has been accepted in ocean engineering (Qiao *et al.*, 1999). The model domain is (23-41°N, 117-132°E) with the horizontal resolution of 1°/6 by 1°/6 including the Bohai Sea, Yellow Sea, East China Sea and the eastern part of the Japan/East Sea as shown in Fig. 1. The wind fields are interpolated into the model grids from NECP (National Centers for Environmental Prediction) reanalyzed data (2001) with the horizontal resolution of 1.25° by 1.0° and the time interval of 6 hours.

### *The MASNUM wave-current coupled model*

Each of the current velocity, temperature and salinity can be separated into two components, a mean part and a fluctuation part (Qiao *et al.*, 2004a),

$$u_{zi} = U_i + u_i,\quad T_z = T + \theta,\quad S_z = S + s \tag{1}$$

where $U_i$, $T$, $S$ are the mean parts, while $u_i$, $\theta$, $s$ represent the fluctuation parts of the velocity, temperature and salinity, respectively, and subscripts $i = 1,2,3$ represent axes of the Cartesian coordinates ($x$, $y$, $z$).

The fluctuation part of velocity can be separated into a turbulence part $u_{ic}$ and a wave-induced fluctuation $u_{iw}$,

$$u_i = u_{iw} + u_{ic} \tag{2}$$

Thus the Reynolds stress can be written as

$$-\langle u_i u_j\rangle = -\langle u_{iw}u_{jw}\rangle - \langle u_{iw}u_{jc}\rangle - \langle u_{ic}u_{jw}\rangle - \langle u_{ic}u_{jc}\rangle \tag{3}$$

where the first term on the right-hand side is the wave-induced Reynolds stress, and the last term can be derived from a turbulence closure model (Mellor and Yamada, 1982) or Prandtl theory (Fang and Ichiye, 1983).

Similarly, the Reynolds diffusivity of temperature and salinity can be written as,

$$-\langle u_i\theta\rangle = -\langle u_{iw}\theta\rangle - \langle u_{ic}\theta\rangle \tag{4}$$

$$-\langle u_i s\rangle = -\langle u_{iw}s\rangle - \langle u_{ic}s\rangle \tag{5}$$

where the last terms on the right-hand side represent the turbulence mixing.

From Prandtl theory, the second, third terms of Eq. (3) and the first terms of Eqs. (4), (5) representing the wave-induced mixing can be expressed as,

$$\{-[\langle u_{iw}u_{jc}\rangle + \langle u_{ic}u_{jw}\rangle]\} = \begin{Bmatrix} 0 & 0 & Bv\dfrac{\partial U_1}{\partial z} \\ 0 & 0 & Bv\dfrac{\partial U_2}{\partial z} \\ Bv\dfrac{\partial U_1}{\partial z} & Bv\dfrac{\partial U_1}{\partial z} & 2Bv\dfrac{\partial U_3}{\partial z} \end{Bmatrix} \tag{6}$$

$$\{-\langle u_{iw}\theta\rangle, -\langle u_{iw}s\rangle\} = \begin{Bmatrix} 0 & 0 \\ 0 & 0 \\ Bv\dfrac{\partial T}{\partial z} & Bv\dfrac{\partial S}{\partial z} \end{Bmatrix} \tag{7}$$

Bv is defined as the wave-induced vertical kinematic viscosity (or diffusivity),

$$Bv = \iint_{\vec{k}} E(\vec{k})\exp\{2kz\}d\vec{k}\frac{\partial}{\partial z}\left(\iint_{\vec{k}} \omega^2 E(\vec{k})\exp\{2kz\}d\vec{k}\right)^{1/2} \tag{8}$$

where $E(\vec{k})$ represents the wave number spectrum, $\omega$,

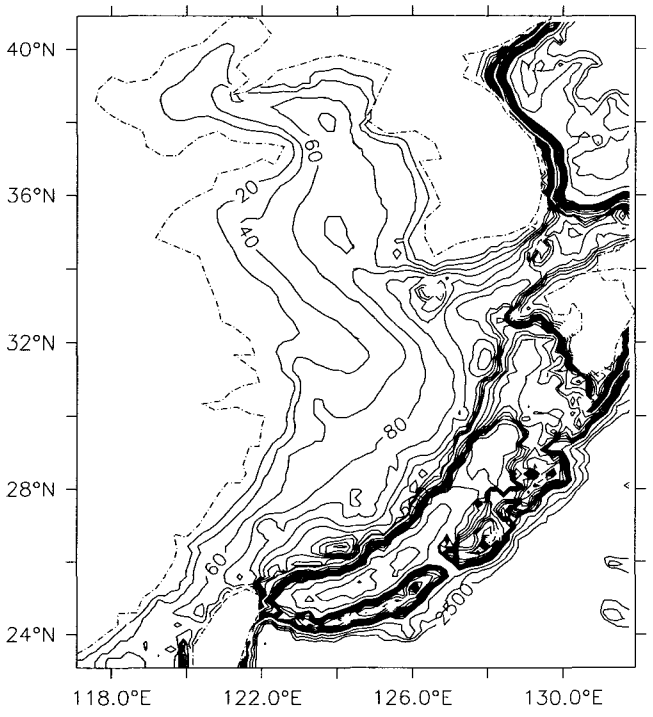


**Fig. 1.** Model domain and topography. Contour interval is 20 m from 0 to 200 m, 100 m from 200 to 1000 m, and 500 m from 1000 to 3000 m.

the wave angular frequency, $k$, wave number, and $z$ is the vertical coordinate axis downward positive with $z = 0$ at the surface. From Eqs. (6) and (7) one can see that parameter Bv is a key factor to determine the wave-induced mixing strength.

### *Circulation model*

Princeton Ocean Model (POM) is adopted in this study with the wave-induced vertical mixing added directly,

$$Km = Km_C + Bv,\ Kh = KhC + Bv \tag{9}$$

where $Km$ and $Kh$ are the vertical viscosity and diffusivity used in the model respectively, $Km_C$ and $Kh_C$ are calculated by the Mellor-Yamada turbulence closure model (Mellor and Yamada, 1982) and Bv is the additional term obtained from the MASNUM wave-current coupled model.

The simulation area is the same as the wave number spectral model. Because the deep ocean is considered unimportant in this paper, the maximal water depth is chosen 3000 m (Fig. 1). 16 vertical layers with a fine resolution in the upper layers are summarized in Table 1.

Same as the wave model, NCEP (2001) offers the sea surface force. Heat flux ($Q$) and the evaporation minus precipitation ($E$-$P$) are from COADS (1994). $Q$ is modified by using the Harney equation (Harney, 1971),

$$Q = Q_c + \left(\frac{dQ}{dt}\right)_c (T_c^0 - T^0) \tag{10}$$

where the subscript c means data from COADS, $T^0$ is the sea surface temperature computed from the circulation model. Scheme provided by POM2k, the $E$-$P$ is added as an equivalent surface salinity flux (Ma and Qiao, 2004),

$$W_S = -(E-P)\times S^0 \tag{11}$$

**Table 1.** Vertical layers of the circulation model

| Layers | σ | Layers | σ |
|---|---|---|---|
| 1 | 0.00000 | 9 | -0.30000 |
| 2 | -0.00313 | 10 | -0.40000 |
| 3 | -0.00625 | 11 | -0.50000 |
| 4 | -0.01250 | 12 | -0.60000 |
| 5 | -0.02500 | 13 | -0.70000 |
| 6 | -0.05000 | 14 | -0.80000 |
| 7 | -0.10000 | 15 | -0.90000 |
| 8 | -0.20000 | 16 | -1.00000 |

where $S^0$ is the surface salinity computed from the model.

The initial and open boundary conditions of salinity are from the Levitus (1982) data set, and those of temperature, and the initial condition of velocity are from the north Pacific simulation results of Xia et al. (2004). To include the tidal current, a radiation condition is fixed for the open boundary velocity and elevation, i.e.

$$\begin{cases} U = U_B - (\pm)\sqrt{\frac{g}{H}}(\zeta_B - \zeta_M) \\ \zeta_B = \zeta_N + \zeta_T \end{cases} \tag{12}$$

where $U_B$ and $\zeta_N$ are from the north Pacific simulation results, $H$, the water depth, $g$, the gravitational acceleration, and $\zeta_M$, the boundary elevation computed from the model. (±) is determined according to the direction outward normal of the open boundary. $\zeta_M$ represents the tidal elevation, i.e.

$$\zeta_T = \sum_i A_i \cos(\omega_i t - \phi_i) \tag{13}$$

Here, the subscript $i$=1 to 8 means the component tide $K_1$, $K_2$, $M_2$, $N_2$, $O_1$, $P_1$, $Q_1$, $S_2$, respectively. ω represents their angular frequency, $A$, amplitude, and ϕ, lag.

The Yangtze River diluted water is included as an estuary across basin boundaries (Ma and Qiao, 2004) by using the climatological monthly mean discharge from a 35-year record at the Datong observation station (Table 2).

Two cases, with and without wave-induced mixing, have been run for five years for stability and the results in the sixth year are compared with the observations.

## DISCUSSION OF MODEL RESULTS

### *Longitudinal transects*

In order to analyze the influence of the vertical diffusivity including wave-induced mixing and tidal mixing on the temperature and salinity in four seasons, the longitudinal transects of relative variables along 36°N in the Yellow Sea are discussed.

**Vertical diffusivity:** February, April, July, and October are chosen as representatives of winter, spring, summer and autumn, respectively. Fig. 2 shows the structures of monthly averaged Bv along 36°N in the

**Table 2.** Climatological monthly mean discharge of the Yangtze River

| Jan. | Feb. | Mar. | Apr. | May | Jun. | Jul. | Aug. | Sep. | Oct. | Nov. | Dec. |
|---|---|---|---|---|---|---|---|---|---|---|---|
| 11008 | 11903 | 16825 | 25254 | 33345 | 40342 | 52183 | 44065 | 39315 | 32952 | 21817 | 13413 |

Units are $m^3/s$.

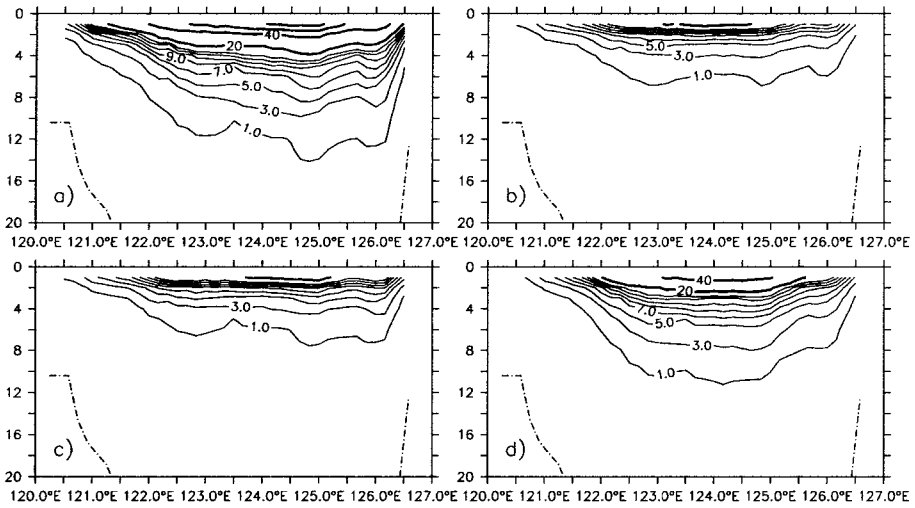


**Fig. 2.** Longitudinal transects of monthly averaged Bv along 36°N in the Yellow Sea. Contour interval is 2 $cm^2\ s^{-1}$ from 1 to 15 $cm^2\ s^{-1}$ (light line), 20 $cm^2\ s^{-1}$ from 20 to 100 $cm^2\ s^{-1}$, and 50 $cm^2\ s^{-1}$ from 100 to 300 $cm^2\ s^{-1}$ (both dark line). (a) Winter, (b) Spring, (c) Summer, (d) Autumn.

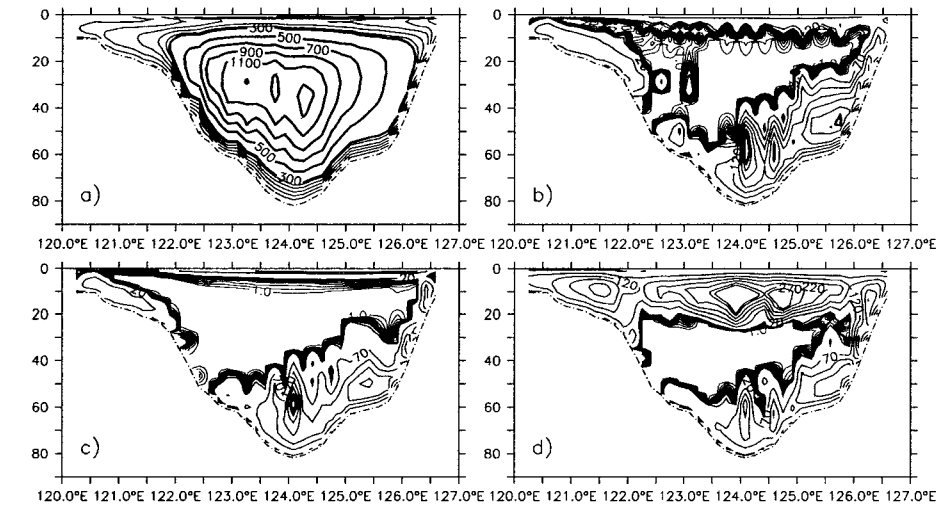


**Fig. 3.** Longitudinal transects of monthly averaged Kh along 36°N in the Yellow Sea. Contour interval is 2 $cm^2\ s^{-1}$ from 1 to 15 $cm^2\ s^{-1}$, 50 $cm^2\ s^{-1}$ from 20 to 270 $cm^2\ s^{-1}$ (both light line), and 200 $cm^2\ s^{-1}$ from 300 to 1500 $cm^2\ s^{-1}$ (dark line). (a) Winter, (b) Spring, (c) Summer, (d) Autumn.

Yellow Sea, which obviously indicates that Bv attenuates downward quickly. Qiao *et al.* (2004b) defined $D_5$, the depth at which Bv decreases to 5 $cm^2\ s^{-1}$, as the wave-induced mixing penetration depth. In winter (Fig. 2a), wave-induced mixing is strongest with the maximum Bv of 100 $cm^2\ s^{-1}$ and $D_5$ of 8.5 m at about 124.8°E. In other three seasons (Figs. 2b, 2c, and 2d), the maximum Bv decreases to 40 $cm^2\ s^{-1}$ at 124°E, 40 $cm^2\ s^{-1}$ at 124.8°E, and 60 $cm^2\ s^{-1}$ at 124.5°E, and that of $D_5$ to 3.5 m, 3.5 m, and 5.4 m in turn.

Because of buoyance-driven mixing, vertical diffusivity in winter is so strong (Fig. 3a) that the wave induced mixing can only make sense near the surface. The maximum of monthly averaged Kh reaches 1400 $cm^2\ s^{-1}$ in the middle part of the transect at the depth of about 40 m. As time goes on, buoyance-driven mixing decreases, so dominance of the wave-induced mixing and tidal mixing emerges. In Figs. 3b and 3c, one can see that tidal mixing is very strong between (120.5°E, 5 m) and (123.5°E, 50 m) and between (123.5°E, 50 m) and (126.5°E, 10 m) where the maximum Kh reaches 550 $cm^2\ s^{-1}$. Although wave-induced mixing is much smaller compared with the tidal mixing, it can dominate the upper ocean mixing. In autumn (Fig. 3d), the upper ocean mixing increases much more than wave-induced mixing. It is believed that buoyance-driven mixing enlarges again.

From Figs. 2 and 3, one can find that both the wave-induced mixing and tidal mixing are stronger in the east than those in the west of the Yellow Sea trough.

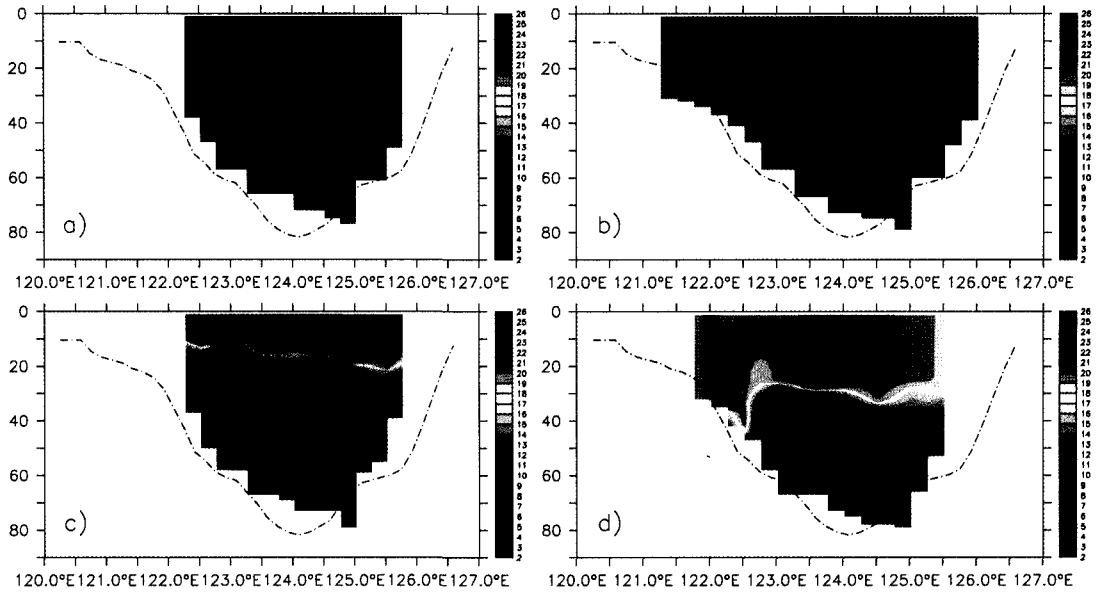


**Fig. 4.** Longitudinal transects of observed temperature along 36°N in the Yellow Sea. (a) Winter, (b) Spring, (c) Summer, (d) Autumn.

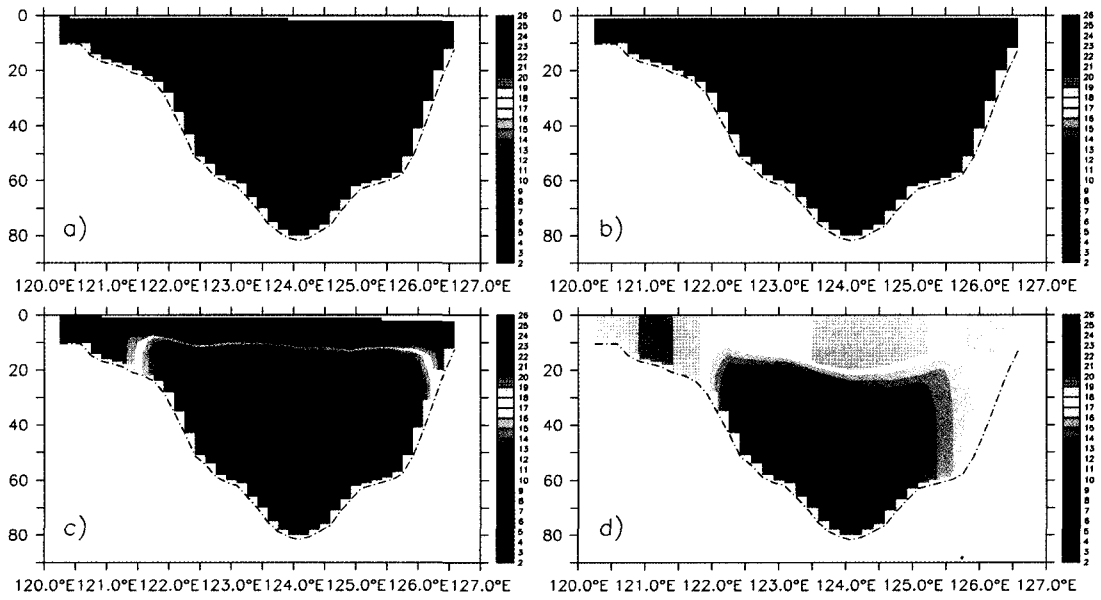


**Fig. 5.** Longitudinal transects of model temperature with wave-induced mixing along 36°N in the Yellow Sea. (a) Winter, (b) Spring, (c) Summer, (d) Autumn.

**Vertical temperature structure:** In this study, the CTD data collected by China-Korea joint cruises in April, October 1996, February and July 1997 are employed to be compared with the model results of which the tidal signals have been removed by a 25 hours average. According to that, the representatives of winter, spring, summer and autumn mentioned above are replaced by February 20th, April 12th, July 16th and October 17th, the approximate cruising dates along the transect, respectively.

Figs. 4, 5, and 6 represent the vertical temperature structures of observations, model results with and without wave-induced mixing, respectively. In winter, temperature is vertically even because of strong mixing. It is believed that the warm kernel between 123°E and 124°E is caused in different response to surface cooling of water in different depth. Three transect are coherent in structure except the 1 °C warmer kernel at 123.6°E in Fig. 6a than in Figs. 4a and 5a. As sea surface heat increases, stratification

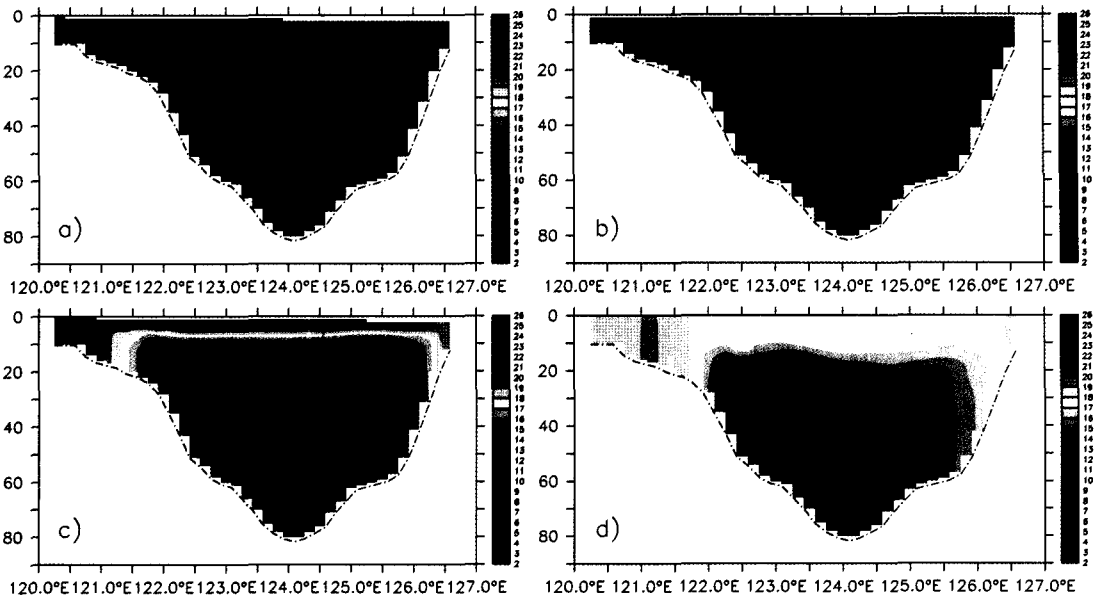


**Fig. 6.** Longitudinal transects of model temperature without wave-induced mixing along 36°N in the Yellow Sea. (a) Winter, (b) Spring, (c) Summer, (d) Autumn.

forms gradually (Figs. 4b, 5b, and 6b). That is also why buoyance-driven mixing decreases. And one can see that the upper mixed layer is forming in both Figs. 4b and 5b, but not in Fig. 6b, which is believed to be caused by wave-induced mixing.

In summer, an upper mixed layer from surface to about 10 m and a strong thermocline fluctuating at the depth between 10 m and 30 m with temperature ranging from 8 °C to 22 °C appear, which is similar in Figs. 4c and 5c. From 125.5°E to 126.5°E in Fig. 5c, there comes the thermocline ventilation which is already confirmed by multi-year averaged data analysis (Chen *et al.*, 1992). Because of limitation of the data collected by China-Korea joint cruises, one can only see that trend in Fig. 4c. It is believed that the strong vertical mixing, especially the tidal mixing mentioned before (Figs. 2c and 3c) in the eastern trough makes the thermocline ventilate. But in Fig. 6c, no upper mixed layer exists and the location, shape and weakness of the thermocline are obviously different from the observations. The only commonness of Figs. 4c, 5c, and 6c is a table structure with fronts located between 120.5°E and 122.5°E and between 125°E and 126.5°E, where tidal mixing is strong. Compared with Figs. 6b and 6c, Figs. 4b, 4c, 5b and 5c show that the wave-induced mixing plays a key role in the formation of the upper mixed layer in spring and summer.

In autumn, as the buoyance-driven mixing enlarging, the thermocline tends to decline. Vertical temperature with wave-induced mixing (Fig. 5d) is more like the observations (Fig. 4d) than that without wave-induced mixing (Fig. 6d).

**Vertical salinity structure:** Vertical salinity transects are shown in Figs. 7, 8, and 9. In winter (Figs. 7a, 8a, and 9a), observations show the same even structure as the model results except for the region between 123°E and 124°E. It seems that the different SSS caused by the error of E-P makes this variance. This error affects the upper ocean so much that only salinity distributions in the deeper water deeper than 40 m are coherent in spring (Figs. 7b, 8b, and 9b).

In summer (Figs. 7c, 8c, and 9c), the simulated upper mixed layer depth and the salinity gradient between 122°E and 124.5°E with wave-induced mixing is more similar to the observations than those without wave-induced mixing. But the halocline in Fig. 7c does not appear in model results.

It is believed that, inaccurate E-P at the resolution of 1° by 1° causes an unacceptable excursion of salinity, which makes the model results different in structure and generally higher than the observations in autumn.

### *Annual cycles*

In order to continuously describe the process of wave-induced mixing in the upper ocean and the formation of the temperature and salinity structure, the

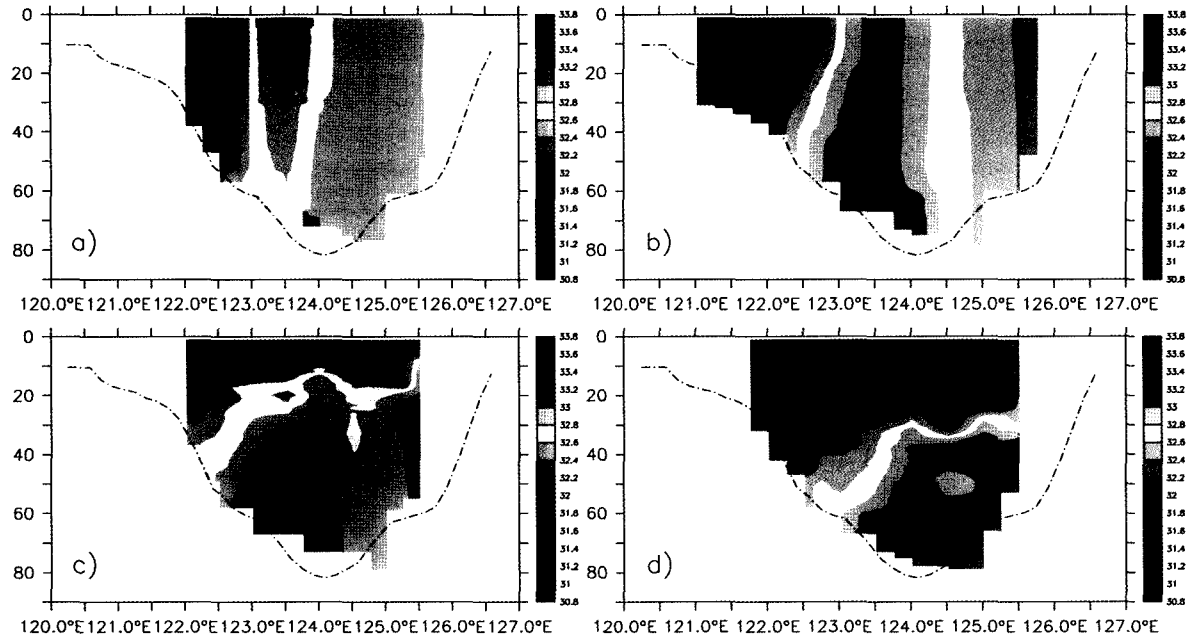


**Fig. 7.** Longitudinal transects of observed salinity along 36°N in the Yellow Sea. (a) Winter, (b) Spring, (c) Summer, (d) Autumn.

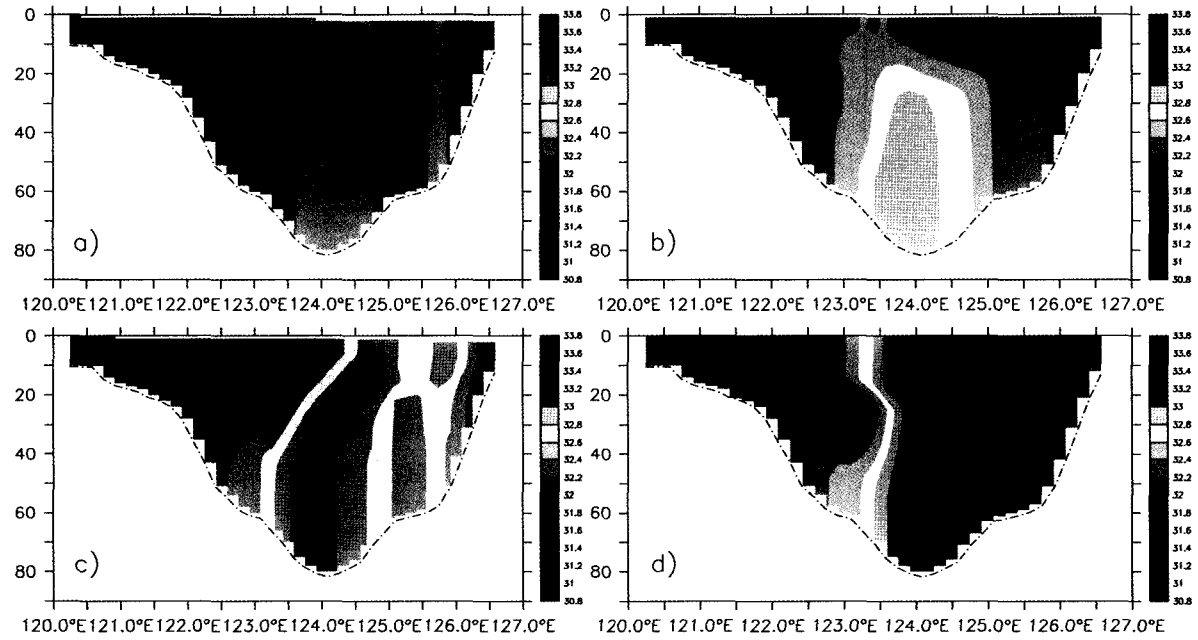


**Fig. 8.** Longitudinal transects of model salinity with wave-induced mixing along 36°N in the Yellow Sea. (a) Winter, (b) Spring, (c) Summer, (d) Autumn.

depth-time images of relative variables at a selected point (125°E, 36°N) are generated.

**Vertical diffusivity:** The annual cycle of Bv at the point (Fig. 10) presents a fluctuation along with the weather condition. One can see that the strongest wave-induced mixing appears from January to March with the maximum Bv of about 300 $cm^2$ $s^{-1}$ and $D_5$ deeper than 14 m in early March. Then Bv and $D_5$ remain relatively low level till late October. Generally, the wave-induced mixing in winter is much stronger than that in summer, which is believed to

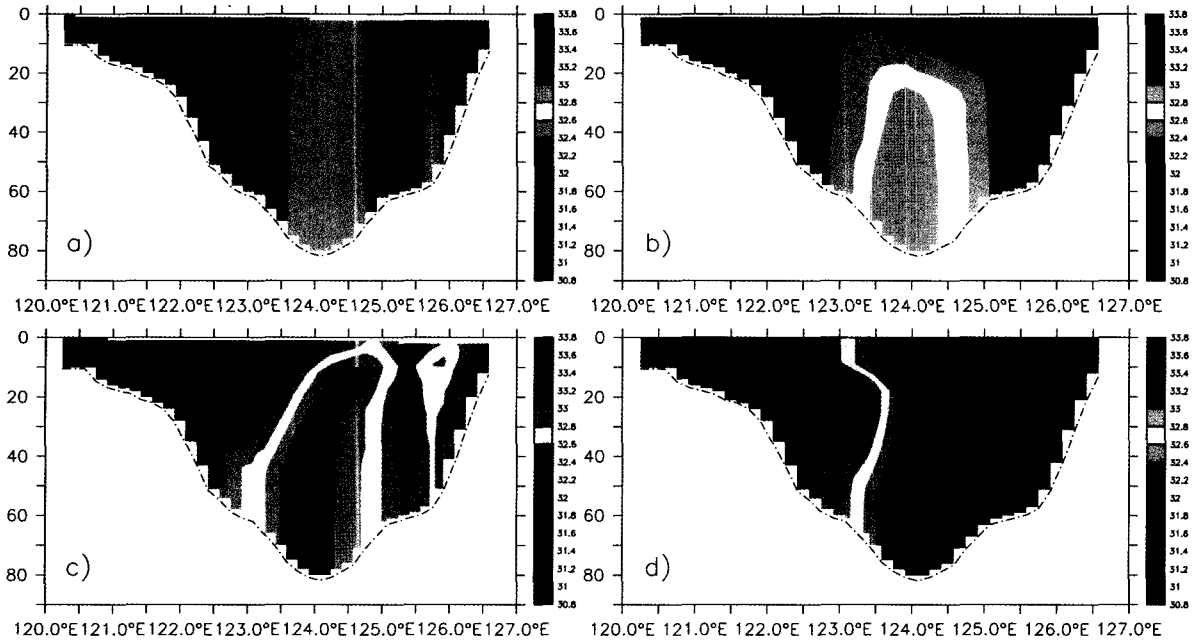


**Fig. 9.** Longitudinal transects of model salinity without wave-induced mixing along 36°N in the Yellow Sea. (a) Winter, (b) Spring, (c) Summer, (d) Autumn.

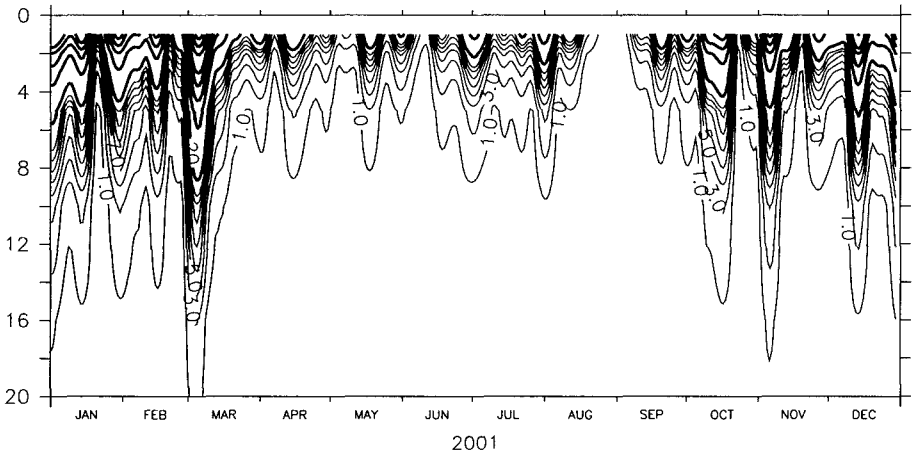


**Fig. 10.** Annual cycle of model Bv at the point (125°E, 36°N). Contour interval is 2 $cm^2 s^{-1}$ from 1 to 15 $cm^2 s^{-1}$ (light line), 20 $cm^2 s^{-1}$ from 20 to 100 $cm^2 s^{-1}$ and 50 $cm^2 s^{-1}$ from 100 to 300 $cm^2 s^{-1}$ (both dark line).

be controlled by the wind stress fields.

Fig. 11 represents the annual cycle of Kh at the point. It can be clearly found that the strongest vertical mixing with the maximum Kh of 3200 $cm^2 s^{-1}$ occurs in late November and December, when buoyance-driven mixing uniforms the density in vertical direction. In comparison with Fig. 10, it can be found that buoyance-driven mixing controls the upper ocean from September to the next March. Then, wave-induced mixing dominates the upper ocean during April and August. In the deeper water deeper than 30 m, vertical diffusivity is mainly controlled by tidal mixing with the maximum Kh of 600 $cm^2 s^{-1}$, which presents quasi half-annual and half-monthly cycles due to tidal periods that are beyond the scope of this study.

**Variability of temperature:** From Fig. 12a, one can see temperature remains vertically even during January and February. The contour of 6 °C between 20 m and 30 m in late February accords with Kh value in the same region, which denotes the early beginning of stratification. In March, buoyance-driven mixing declines gradually, and in April, the upper ocean mixed layer and thermocline begin to form. In comparison with Fig. 11, one can find that both the wave-induced mixing and tidal mixing play key roles in the forming period of the thermocline, upper and lower mixed layers from April to mid June

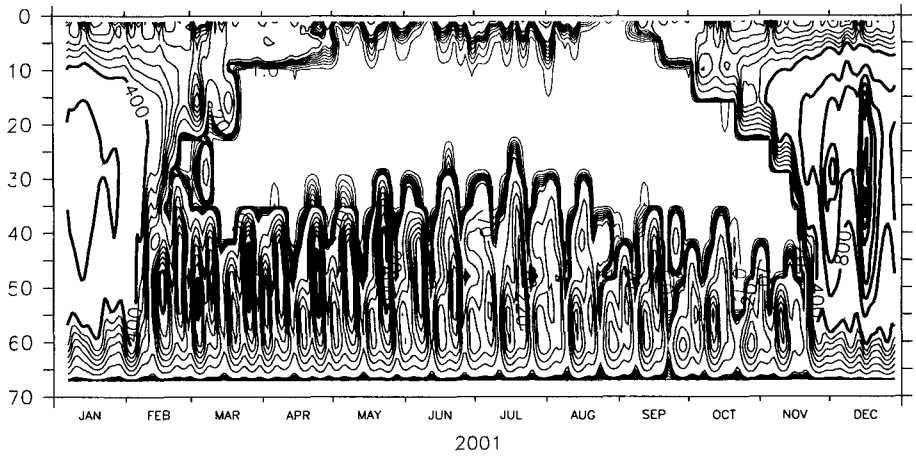


**Fig. 11.** Annual cycle of model Kh at the point (125°E, 36°N). Contour interval is 2 $cm^2\ s^{-1}$ from 1 to 15 $cm^2\ s^{-1}$, 50 $cm^2\ s^{-1}$ from 20 to 320 $cm^2\ s^{-1}$ (both light line), and 400 $cm^2\ s^{-1}$ from 400 to 3200 $cm^2\ s^{-1}$ (dark line).

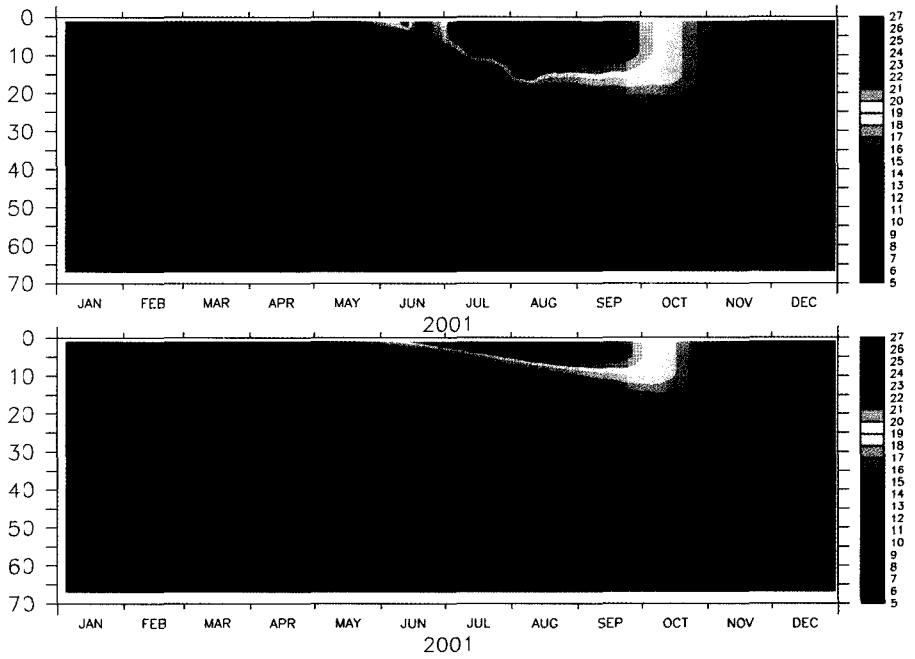


**Fig. 12.** Annual cycles of model temperature at the point (125°E, 36°N). (a) With wave-induced mixing, (b) Without wave-induced mixing.

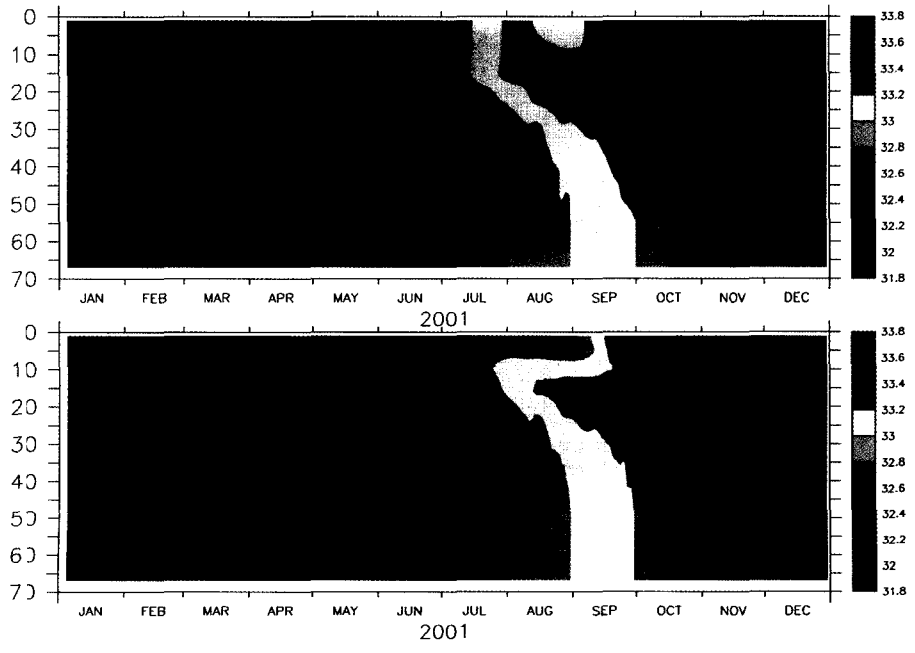


**Fig. 13.** Annual cycles of model salinity at the point (125°E, 36°N). (a) With wave-induced mixing, (b) Without wave-induced mixing.

and in the maintaining period from mid June to August. In September, as the buoyance-driven mixing increasing, the mixed layer begins to thicken, the thermocline begins to decline and finally, vertical temperature is uniformed in late November.

Fig. 12b shows the temperature variability without wave-induced mixing. Great difference is found during April and September. One can clearly see that without wave-induced mixing, the upper ocean mixed layer cannot form in spring and summer, and the thermocline would be shallower and weaker as mentioned before.

**Variability of salinity:** The excursion of salinity caused by inaccurate E-P mentioned before can be seen in Fig. 13, which is going to be dealt with in future study.

## CONCLUSIONS

1. Wave-induced vertical kinematic viscosity (or diffusivity) coefficient Bv is derived and calculated from the MASNUM wave number spectral model to determine the wave-induced mixing strength. Longitudinal transects and depth-time images show that Bv attenuates quickly in vertical direction and is strongest in winter and weakest in autumn.

2. Comparisons between the observations and MASNUM wave-current coupled model results of temperature and salinity along 36°N in the Yellow Sea indicate that it is the wave-induced mixing that greatly help the formation of the mixed layer and thermocline in spring and summer. Tidal mixing and wave-induced mixing are responsible for the thermocline ventilation in the east of the Yellow Sea. Buoyance-driven mixing plays a key role in the vertical uniformity in winter.

## ACKNOWLEDGEMENT

This study is supported by the national key basic research program under contract G1999043809.

## REFERENCES

Blumberg, A.F. and G.L. Mellor, 1987. A description of a three-dimensional coastal ocean model. *Three dimensional coastal ocean models*, N. S. Heaps, Editor, American Geophysical Union, Washington D. C., 1–16.

Chen, G. *et al.*, 1992. *Marine atlas of the Bohai Sea, Yellow Sea and East China Sea, Hydrology.* China Ocean Press, Editor, Editorial Board for Marine Atlas, Beijing, **524**: 247–255 (In Chinese).

Craig, P.D. and M.L. Banner, 1994. Modeling wave-enhanced turbulence in the ocean surface layer. *J. Phys. Oceanogr.*, **24**: 2546–2559.

Ezer, T., 2000. On the seasonal mixed layer simulated by a basin-scale ocean model and the Mellor-Yamada turbulence scheme. *J. Geophys. Res.*, **105**(C7): 16843–16855.

Fang, G. and T. Ichiye, 1983. On the vertical structure of tidal currents in a homogeneous sea. *Geophys. J. R. Astr. Soc.*, **73**: 65–82.

Harney, R., 1971. Surface thermal boundary condition for ocean circulation models. *J. Phys. Oceanogr.*, **1**: 241–248.

Kantha, L.H. and C.A. Clayson, 1994. An improved mixed layer model for geophysical applications. *J. Geophys. Res.*, **99**: 25235–25266.

Lee, S.H. and R.C. Beardsley, 1999. Influence of stratification on residual tidal currents in the Yellow Sea. *J. Geophys. Res.*, **104**(C7): 15679–15701.

Levitus, S., 1982. Climatological atlas of the world ocean. *NOAA Prof. Paper* No. 13. U. S. Govt. Printing Office, 173 pp. plus 17 microfiche.

Liungman, O., 2000. Tidally forced internal wave mixing in a $\kappa$–$\varepsilon$ model framework applied to Byfjorden basins. *J. Phys. Oceanogr.*, **30**: 352–368.

Ma, J. and F. Qiao, 2004. Simulation and analysis on the seasonal variability of salinity in the Yellow Sea. (Submitted to *J. Oceanogr.*)

Martin, P.J., 1985. Simulation of the mixed layer at OWS November and Papa with several models. *J. Geophys. Res.*, **90**: 581–597.

Mellor, G.L., 2001. One-dimensional, ocean surface layer modeling. a problem and a solution. *J. Phys. Oceanogr.*, **31**: 790–809.

Mellor, G.L. and T. Yamada, 1982. Development of a turbulence closure model for geophysical fluid problems. *Rev. Geophys. and Space Phys.*, **20**: 851–875.

Pacanowski, R.C. and S.G.H. Philander, 1981. Parameterization of vertical mixing in numerical models of tropical oceans. *J. Phys. Oceanogr.*, **11**: 443–451.

Qiao, F., S. Chen, C. Li, W. Zhao and Z. Pan, 1999. The study of wind, wave, current extreme parameters and climatic characters of the South China Sea. *Journal of Marine Technology Society*, **33**(1): 61–68.

Qiao, F., Y. Yuan, T. Ezer, C. Xia, Y. Yang and J. Ma, 2004a. A three-dimensional, surface wave-ocean circulation coupled model: System description and initial testing. (Submitted to *J. Phys. Oceanogr.*)

Qiao, F., Y. Yuan, Y. Yang, Q. Zheng, C. Xia and J. Ma, 2004b. Wave-induced mixing in the upper ocean: Distribution and application to a global ocean circulation model. (Submitted to *Geophys. Res. Lett.*)

Xia, C., F. Qiao and Y. Yuan, 2004. Numerical simulation of the general circulation. (In Chinese; Submitted to *Chinese Journal of Computational Physics.*)

Yang, Y. and F. Qiao, 2004. The description of the MASNUM numerical wave model. (Accepted by *Chin. J. Oceanol. Limnol.*)

Yu, W., F. Qiao, Y. Yuan and Z. Pan, 1997. Numerical modeling of wind and waves for Typhoon Betty (8710). *Acta Ocenologica Sinica*, **16**(4): 459–473.

Yuan, Y., Z. Pan, F. Hua, L. Sun, 1991. LAGDF-WAM numerical wave model. *Acta Ocenologica Sinica*, **10**: 483–488.

Yuan, Y., F. Qiao, F. Hua and Z. Wan, 1999. The development of a coastal circulation numerical model: 1. Wave-induced mixing and wave-current interaction. *J. Hydrodynamics*, Ser. A. **14**(4B):

1–8 (In Chinese).

Yuan, Y. and H. Li, 1993. Research on the circulation structure and forming mechanism of the Yellow Sea cold water mass. *Science in China*, **23**(1): 93–103 (In Chinese).

Yuan, Y., F. Qiao and D. Dai, 2003. Governing equations of oceanic internal waves. *Advances in Marine Science*, **21**(3): 243–250. (In Chinese).

Manuscript received October 15, 2003
Revision accepted February 15, 2004
Editorial handling: Chang S. Kim